

Abstract

The record-breaking major stratospheric warming of northern winter 2009 (January–February) is studied using BASCOE (Belgian Assimilation System for Chemical Observation) stratospheric water vapour analyses and MLS (Microwave Limb Sounder) water vapour observations, together with meteorological data from the European Centre for Medium-Range Weather Forecasts (ECMWF) and potential vorticity derived from ECMWF meteorological data. We focus on the interaction between the cyclonic wintertime stratospheric polar vortex and subsidiary anticyclonic stratospheric circulations during the build-up, peak and aftermath of the major warming. We show dynamical consistency between the water vapour analysed fields, and the meteorological and PV fields. New results include the analysis of water vapour during the major warming and demonstration of the benefit of assimilating MLS satellite data into the BASCOE model.

1 Introduction

The main feature of the wintertime stratosphere is a strong cyclonic polar vortex that organizes the stratospheric flow; anticyclonic circulations are also commonly present (Lahoz et al., 2009 and references therein). The Arctic and Antarctic winter stratosphere can be described in terms of vortex interactions between a dominant cyclonic polar vortex and one or more subsidiary anticyclones. These wintertime anticyclones can be: (i) quasi-stationary, e.g., the Aleutian High in Arctic winter (Lahoz et al., 1994; Harvey et al., 2002); a climatological anticyclone to the South of Australia in late Antarctic winter (Mechoso et al., 1988; Lahoz et al., 1996, 2006; Harvey et al., 2002, 2004); or (ii) travelling, e.g., eastward travelling anticyclones in mid Antarctic winter, vortex mergers during Arctic and Antarctic winter (Lahoz et al., 1996; Manney et al., 2005).

A particularly interesting dynamical event in the Arctic wintertime stratosphere is the major stratospheric warming (see, e.g., Charlton and Polvani, 2007). These events

ACPD

10, 24699–24734, 2010

The 2009 stratospheric major warming

W. A. Lahoz et al.

Title Page

Abstract

Introduction

Conclusions

References

Tables

Figures

◀

▶

◀

▶

Back

Close

Full Screen / Esc

Printer-friendly Version

Interactive Discussion



dramatically disrupt the typical wintertime circulation of the stratosphere. They can also affect tropospheric weather patterns (e.g. Baldwin and Dunkerton, 2001). Climate change induced changes in the frequency and characteristics of major stratospheric warmings are expected owing to changes in the Brewer-Dobson circulation; such changes will in turn impact stratospheric ozone loss and recovery, and tropospheric climate (e.g. WMO, 2007; Charlton-Perez et al., 2008). Major warmings can be classified as vortex displacement (also wavenumber-1) or vortex split (also wavenumber-2) events. During these events the polar vortex is strongly disrupted, and in the mid stratosphere (e.g. 10 hPa) polar temperatures increase dramatically over a few days and zonal mean zonal winds reverse sign from westerly to easterly at latitudes poleward of 60° N.

The major warming that took place during January–February 2009 was the strongest and most prolonged on record (Labitzke and Kunze, 2009; Manney et al., 2009b); it was a vortex-split event, and major stratospheric warming criteria were met on 24 January: easterly zonally averaged zonal winds at 10 hPa and 60° N, and temperature gradient reversal poleward of 60° N at 10 hPa. Only in the past few years have sufficient data been available to thoroughly study the dynamics and transport during a major stratospheric warming throughout the upper troposphere to the mesosphere – see Manney et al. (2009b) and references therein for details. These papers have studied major stratospheric warmings based on observations of tracers, meteorological analyses of geopotential height, temperature and horizontal winds, and fields of potential vorticity (PV) derived from meteorological analyses. However, to our knowledge, major warmings have not been studied hitherto using analyses of stratospheric water vapour produced using data assimilation, chiefly because it is only recently that such analyses have started to become available and be evaluated (Lahoz et al., 2007a, b; Thornton et al., 2009).

We use stratospheric water vapour analyses and observations synergistically to study the spatial characteristics and temporal evolution of the cyclonic and anticyclonic circulations prevalent during the major stratospheric warming that took place

The 2009 stratospheric major warming

W. A. Lahoz et al.

[Title Page](#)[Abstract](#)[Introduction](#)[Conclusions](#)[References](#)[Tables](#)[Figures](#)[⏪](#)[⏩](#)[◀](#)[▶](#)[Back](#)[Close](#)[Full Screen / Esc](#)[Printer-friendly Version](#)[Interactive Discussion](#)

during January–February 2009. Water vapour analyses are from the state-of-the-art BASCOE (Belgian Assimilation System for Chemical Observations) chemical data assimilation system (Errera and Fonteyn, 2001; Errera et al., 2008; Viscardy et al., 2010). Water vapour observations are from MLS, the Microwave Limb Sounder (Lambert et al., 2007). These data are supplemented with meteorological data (geopotential height) from the European Centre for Medium-Range Weather Forecasts, ECMWF (Simmons et al., 2005), and PV fields from ECMWF meteorological data. These ECMWF data come from the ERA Interim analyses (<http://www.ecmwf.int/research/era/do/get/index>).

Data used in this paper are analysed using a 1-D along-orbit picture (see Lahoz et al., 2009, and references therein) and a 2-D equivalent latitude-theta picture, where theta is potential temperature (see Manney et al., 2009b, and references therein). Data are also analysed with 2-D latitude-longitude maps at selected pressure or theta levels. The geometry of the 1-D picture provides a physically meaningful (coordinate independent) pole-centred picture of the stratosphere and mesosphere. An advantage of the pole-centred picture is that it retains the information content in the data without the blurring effect of gridding by interpolation between viewing tracks and averaging along latitude circles. The 2-D equivalent latitude-theta picture involves some interpolation and averaging, but since the averaging is done along PV contours, preserves much of the vortex-centred viewpoint; this view provides information on the roles of quasi-horizontal transport and vertical transport in determining tracer distributions.

It can be advantageous to fill in the observational gaps between the viewing tracks, for example, to estimate ozone loss, and compute vortex-averaged quantities of tracers that can be used to estimate vertical transport (e.g. identified by descent of tracer isopleths). An objective method to fill in the observational gaps is data assimilation (see, e.g., Lahoz et al., 2010). This combines the information from the observations and the a priori knowledge of the state of the atmosphere (and their associated error covariances), the latter typically embodied in a numerical model. Data assimilation has been used successfully to produce analyses of stratospheric constituents such as ozone and water vapour; evaluate observations of stratospheric chemical constituents;

The 2009 stratospheric major warming

W. A. Lahoz et al.

[Title Page](#)[Abstract](#)[Introduction](#)[Conclusions](#)[References](#)[Tables](#)[Figures](#)[⏪](#)[⏩](#)[◀](#)[▶](#)[Back](#)[Close](#)[Full Screen / Esc](#)[Printer-friendly Version](#)[Interactive Discussion](#)

and evaluate chemical models. Papers describing this work include Geer et al. (2006, 2007), Lahoz et al. (2007a, b) and Thornton et al. (2009). The review by Lahoz et al. (2007a) includes a comprehensive list of further references. Data assimilation has also been used to estimate stratospheric ozone loss (see, e.g., Jackson and Orsolini, 2008; El Amraoui et al., 2008; Rösevall et al., 2008; the World Meteorological Office, WMO, website, <http://www.wmo.int/pages/prof/arep/gaw/ozone/index.html>).

Section 2 describes the BASCOE chemical data assimilation system and the MLS water vapour data. Section 3 presents the winter evolution from the point of view of the BASCOE analyses. Sections 4–5 describe the evolution of the stratosphere for selected dates during the January–February 2009 period, spanning the build-up, peak and aftermath of the major warming. Section 4 provides a picture of the meteorology from ECMWF data. Section 5 provides, first, a comparison of 2-D water vapour analyses and 2-D gridded MLS water vapour observations, with a focus on the added value of the data assimilation method compared to observations (Sect. 5.1); second, a combined 2-D maps/1-D along-orbit pole-centred picture of the dynamics, looking at water vapour observations and analyses, and PV fields, with a focus on the consistency of the different dynamical pictures of the major warming (Sect. 5.2); and third, 2-D equivalent latitude-theta maps of the BASCOE water vapour analyses and BASCOE chemistry transport model (CTM) simulations, with a focus on representation of transport processes during the major warming (Sect. 5.3). The MLS orbits considered in Sect. 5.2 are chosen to cut through the cyclonic and anticyclonic circulations present during the period of the major warming. Section 6 discusses results in Sects. 3–5. Section 7 provides conclusions. New results in this paper include the analysis of water vapour during the major warming and demonstration of the benefit of assimilating MLS satellite data into the BASCOE model.

The 2009 stratospheric major warming

W. A. Lahoz et al.

[Title Page](#)[Abstract](#)[Introduction](#)[Conclusions](#)[References](#)[Tables](#)[Figures](#)[Back](#)[Close](#)[Full Screen / Esc](#)[Printer-friendly Version](#)[Interactive Discussion](#)

2 BASCOE data assimilation system

2.1 BASCOE set-up

BASCOE is a 4D-Var (4-d variational) assimilation system described in Errera et al. (2008). Its performance for various analysed species is described in several papers (Errera and Fonteyn, 2001; Geer et al., 2006; Lahoz et al., 2007b; Errera et al., 2008; Thornton et al., 2009; Viscardy et al., 2010). The BASCOE system is based on a 3-D CTM dedicated to stratospheric chemistry processes; it uses a time step of 30 minutes. In this study, the CTM is driven by ECMWF ERA Interim analyses of winds and temperatures on a subset of 37 of the 60 ECMWF model levels, from the surface to 0.1 hPa with a horizontal resolution set to 3.75° longitude by 2.5° latitude. Hence, the horizontal resolution corresponds to a maximum of ~415 km in longitude and a maximum of ~277 km in latitude. The vertical resolution is ~1.5 km in the mid stratosphere.

The BASCOE CTM includes a parametrization to take into account the effect of Polar Stratospheric Clouds (PSCs) – see Errera et al. (2008) for details. Although the BASCOE model extends down to the surface, it does not include any tropospheric processes. Below the tropopause, MLS water vapour profiles are not assimilated as the BASCOE model fixes the tropospheric water vapour field to that of the ECMWF ERA Interim analyses. The thermal tropopause is calculated in the BASCOE model using ECMWF ERA Interim pressure and temperature fields mapped to the BASCOE horizontal resolution.

For the experiments described in this paper, the BASCOE system assimilates over a 24-hour window various MLS version v2.2 species within their useful vertical range (see Table 1.1 in the v2.2 Data Quality Document, Livesey et al., 2007). These species are: H₂O, ClO, HCl, HNO₃, N₂O, O₃ and OH. CO and N₂O observations are used by Manney et al. (2009b) to study the major warming of 2009. This was possible by considering averages of these observations. In data assimilation observations are considered individually, and the relatively large observation errors bars of MLS CO and

The 2009 stratospheric major warming

W. A. Lahoz et al.

Title Page

Abstract

Introduction

Conclusions

References

Tables

Figures

◀

▶

◀

▶

Back

Close

Full Screen / Esc

Printer-friendly Version

Interactive Discussion



N₂O compared to the BASCOE background error (see below) – for CO over the whole vertical domain of BASCOE (Pumphrey et al., 2007), for N₂O above 10 hPa (Lambert et al., 2007) – mean their weight in the analyses is insignificant. We thus exclude these species from this study. Instead, to study the major warming, we use the MLS water vapour observations and the BASCOE water vapour analyses. Their validation is discussed in Sects. 2.2 and 2.3, respectively.

Water vapour is a control variable in the BASCOE 4D-Var system and the BASCOE background errors are diagonal (i.e., all off-diagonal elements are set to zero) with a standard deviation equal to 20% of the background humidity field.

2.2 Validation of MLS water vapour observations

The MLS v2.2 water vapour data have been validated by Lambert et al. (2007). Single-profile precision is ~0.2–0.3 parts per million by volume, ppmv (4–9%) and vertical resolution is ~3–4 km in the stratosphere. Precision and vertical resolution gets worse with increasing height above the stratopause. Over the pressure range 0.1 hPa–0.01 hPa precision degrades from ~0.4 ppmv to ~1.1 ppmv (6% to 34%) and vertical resolution degrades to ~12–16 km. Accuracy is estimated to be 0.2–0.5 ppmv (4–11%) for the pressure range 68 hPa–0.01 hPa. The scientifically useful range of the data is from 316 hPa to 0.002 hPa.

2.3 Validation of BASCOE water vapour analyses

The BASCOE stratospheric water vapour analyses have been verified against water vapour data from MLS (a self-consistency test), and validated against independent water vapour data from the ACE-FTS (Atmospheric Chemistry Experiment-Fourier Transform Spectrometer) instrument (Bernath et al., 2005). Figure 1 shows a comparison between the BASCOE water vapour analyses, and the MLS and ACE-FTS water vapour data, averaged for the period January–February 2009 and over the latitude range 60° N–90° N. From Fig. 1, bias differences between BASCOE and MLS

The 2009 stratospheric major warming

W. A. Lahoz et al.

Title Page

Abstract

Introduction

Conclusions

References

Tables

Figures

◀

▶

◀

▶

Back

Close

Full Screen / Esc

Printer-friendly Version

Interactive Discussion



are less than 2% throughout the stratosphere, and bias differences between BASCOE and ACE-FTS are less than 5% throughout the stratosphere. BASCOE is slightly drier than ACE-FTS in the mid to upper stratosphere (10 hPa–1 hPa), and slightly moister in the lower stratosphere, chiefly around 50 hPa. The standard deviation difference between BASCOE analyses and both MLS and ACE-FTS data, is typically less than 7% throughout the stratosphere (100 hPa–1 hPa), with values being less than 5% in the mid and upper stratosphere (10 hPa–1 hPa). The bias and standard deviation differences between BASCOE and MLS are within the precision of the latter (see Sect. 2.2).

3 Water vapour analyses: temporal evolution during winter 2009

We present, for the period 1 January–28 February 2009, a time series of the vortex-averaged water vapour throughout the stratosphere and lower mesosphere (400 K–2000 K) computed from analyses (Fig. 2, top), and a BASCOE CTM simulation without assimilation and including chemistry (Fig. 2, bottom). The vortex edge is defined using the $1 \times 10^{-4} \text{ s}^{-1}$ scaled PV (sPV) discussed in Manney et al. (2007). The white area in Fig. 2 corresponds to the region where the vortex is not defined according to this criterion. Using PV fields derived from GEOS-5 shows no significant differences in the results (not shown). A BASCOE CTM simulation without assimilation and without chemistry was also done, with results very similar to those including chemistry (not shown), indicating that advection and not chemistry is the dominant process during the period of the major warming. Comparison of the BASCOE CTM (run without assimilation) against independent data (ACE-FTS) shows that in the stratosphere the model has a positive bias (within 5%) and that differences have a standard deviation within 10%. In general, in this comparison, the BASCOE CTM performs worse than the BASCOE analyses, although differences are small (between 2% and 5%).

The BASCOE water vapour analyses show three notable features: (i) an air mass characterized by water vapour mixing ratios of ~ 6 ppmv (yellow-green colours in Fig. 2, top), present in the lower mesosphere (2000 K) during early and mid January, which

The 2009 stratospheric major warming

W. A. Lahoz et al.

Title Page

Abstract

Introduction

Conclusions

References

Tables

Figures

◀

▶

◀

▶

Back

Close

Full Screen / Esc

Printer-friendly Version

Interactive Discussion



descends to the mid stratosphere (1000 K) by 24 January (the date major warming criteria were met), with descent appearing to stop abruptly (there is, through most of the vertical range and time period considered, still diabatic descent taking place, but strong mixing as the vortex breaks up destroys the signature of confined descent in the tracer fields); (ii) an air mass characterized by water vapour mixing ratios greater than 6.5 ppmv (red colours in Fig. 2, top), present in the mid stratosphere (~800 K) during early January, which descends to the mid/lower stratosphere (~700 K) by 1 February and then stalls; and (iii) an air mass characterized by water vapour mixing ratios greater than 6.5 ppmv (red colours in Fig. 2, top), present in the lower mesosphere (~1900 K) in 20 January, which descends to the upper stratosphere (~150 K) by 15 February, with descent stalled afterwards. The origins of these features and their relationship to the major warming are discussed below. In Sects. 4–5 we look in more detail at selected dates during the period of the major warming.

The vortex average calculated from the CTM run (Fig. 2, bottom) generally shows the same broad-scale features as the vortex average calculated from the BASCOE analyses (Fig. 2, top), but shows differences in the representation of localized features. The CTM-based estimate shows higher mixing ratios in the mid and upper stratosphere, and lower mixing ratios in the mid and lower stratosphere during the peak of the major warming (20–24 January), and shows higher mixing ratios in the upper stratosphere in the period after the major warming (late January/February). These differences are typically of order 0.25–0.5 ppmv. As the localized features seen in the BASCOE analyses are consistent with the meteorological data (see Manney et al., 2009b, and confirmed by results shown in Sect. 5.3), we infer vortex-averaged estimates calculated from the BASCOE analyses are more realistic than those calculated from the CTM runs (with and without chemistry). This suggests that forcing a CTM with ECMWF winds and diabatic heating corresponding to the ERA Interim analyses (and not using data assimilation) produces polar vortex tracer fields (dependent on transport and not chemistry) with a positive bias of order 0.25–0.5 ppmv.

The 2009 stratospheric major warming

W. A. Lahoz et al.

[Title Page](#)[Abstract](#)[Introduction](#)[Conclusions](#)[References](#)[Tables](#)[Figures](#)[Back](#)[Close](#)[Full Screen / Esc](#)[Printer-friendly Version](#)[Interactive Discussion](#)

The 2009 stratospheric major warming

W. A. Lahoz et al.

Title Page

Abstract

Introduction

Conclusions

References

Tables

Figures

◀

▶

◀

▶

Back

Close

Full Screen / Esc

Printer-friendly Version

Interactive Discussion



The first feature identified in Fig. 2 (top) is associated with typical early winter diabatic descent in the polar vortex (Manney et al., 1994, 2009a, b). This confined descent brings relatively dry mesospheric air to the mid stratosphere, where the ambient air is moister. Figure 2 in Manney et al. (2009b) shows similar strong descent in the MLS CO observations. Focusing on H₂O mixing ratios of ~6 ppmv, these isopleths descend (although not in a coherent fashion) from 2000 K on 8 January to ~1300 K on 22 January, and appear to stop abruptly at ~1000 K on 24 January, when major warming criteria were met and the vortex split in the mid stratosphere (Manney et al., 2009b), resulting in strong mixing that eliminated the signature of confined descent. This gives a descent rate of the isopleths of ~60 K day⁻¹ or, alternatively, ~1 km day⁻¹ (50 km to 35 km in 16 days). An alternative approach focusing on the green contour (isopleths less than 6 ppmv) shows descent from 2000 K (12 January) to ~1500 K (25 January), a descent rate of ~40 K day⁻¹. This suggests descent rates for this air mass between 40 K day⁻¹ and 60 K day⁻¹. Here and elsewhere in the paper, descent rates are in terms of d(theta)/dt. In Sect. 5.3 we use the equivalent latitude-theta picture to revisit estimates of descent rates based on BASCOE water vapour analyses.

The second feature identified in Fig. 2 (top) is associated with descent before the major warming (24 January) and the subsequent vortex split in the mid and mid/lower stratosphere (Manney et al., 2009b). This air does not mix with the relatively drier air of mesospheric origin immediately above. This descent of air brings relatively moist mid/upper stratospheric air to the mid stratosphere, where the ambient air is drier. Figure 2 in Manney et al. (2009b) shows similar descent in the MLS N₂O observations. Focusing on H₂O mixing ratios of 6.5 ppmv, these isopleths descend from ~1000 K in 1 January to ~800 K by 9 February; after this time the isopleths stall and stop descending. This implies a descent rate of ~5 K day⁻¹ for this air mass. An alternative approach focusing on the red contours greater than 6.5 ppmv shows descent from 850 K (1 January) to ~750 K (22 January), also a descent rate of ~5 K day⁻¹ (~30 km to ~20 km over 20 days, a descent rate of ~0.5 km day⁻¹). During this descent, and especially after the peak of the warming in 24 January, the region of locally high mixing ratios (e.g.

values greater than 6.5 ppmv) decreases, suggesting mixing between extra-vortex and vortex air as the vortex splits.

The third feature identified in Fig. 2 (top) is associated with strong descent after the major warming (24 January) and subsequent reformation of the vortex in the upper stratosphere/mesosphere (Manney et al., 2009b). This descent of air brings relatively moist upper stratosphere/mesosphere air to the mid stratosphere, where the ambient air is drier. Figure 2 in Manney et al. (2009b) shows similar strong descent in the MLS CO observations. Focusing on H₂O mixing ratios of 6.5 ppmv, these isopleths descend from 2000 K on 20 January to ~1500 K on 10 February; after this time the isopleths stop descending. This implies a descent rate of ~25 Kday⁻¹ (~50 km to ~40 km over 20 days, a descent rate of ~0.5 kmday⁻¹) for this air mass. An alternative approach focusing on isopleths greater than 7 ppmv (red colours) shows descent from ~1900 K (25 January) to ~1500 K (14 February), a descent rate of ~20 K day⁻¹. This suggests descent rates for this air mass between 20 Kday⁻¹ and 25 K day⁻¹.

We now compare the descent rates estimated above with estimates based on Fig. 2 of Manney et al. (2009b), where we consider the motion of tracer isopleths of CO and N₂O. Note, however, that a comparison which considers the motion of tracer isopleths of different tracers (as done here) is likely to incur errors due to different strengths in the horizontal gradients of the tracers. In particular, since N₂O and CO have stronger horizontal gradients in the stratosphere/lower mesosphere than water vapour, horizontal mixing would tend to modify these fields more significantly and mask the extent of the vertical descent within the vortex more than for water vapour. This would result in larger descent rates estimated using water vapour than those estimated from Manney et al. (2009b).

From Fig. 2 of Manney et al. (2009b) we estimate the following descent rates: (i) 700 ppbv (parts per billion by volume) CO isopleth from ~2000 K (8 January) to ~1500 K (24 January), a descent rate of ~30 K day⁻¹ (compare with the estimate of ~40 K day⁻¹ to ~60 K day⁻¹ from the vortex averaged quantity); (ii) 40 ppbv N₂O isopleth from ~700 K (early January) to ~600 K (late January), a descent rate of ~3 K day⁻¹ (compare with

**The 2009
stratospheric major
warming**

W. A. Lahoz et al.

Title Page

Abstract

Introduction

Conclusions

References

Tables

Figures

◀

▶

◀

▶

Back

Close

Full Screen / Esc

Printer-friendly Version

Interactive Discussion



the estimate of $\sim 5 \text{ K day}^{-1}$ from the vortex averaged quantity); and (iii) 350 ppbv CO isopleth from $\sim 2200 \text{ K}$ (late January) to $\sim 2000 \text{ K}$ (mid February), a descent rate of $\sim 20 \text{ K day}^{-1}$ (compare with the estimate of $\sim 20 \text{ K day}^{-1}$ to $\sim 25 \text{ K day}^{-1}$ from the vortex averaged quantity). The results from the vortex-averaged quantities in Fig. 2 (top) agree qualitatively with those from Manney et al. (2009b) in the nature and timing of the descent (descent of mesospheric air to the mid stratosphere up to the time of the major warming, which then appears to stop abruptly), but tend to overestimate the descent rate based on Manney et al. (2009b). This is to be expected given the different characteristics of the horizontal gradients of CO, N_2O and water vapour (see above). Overall, given these caveats, the estimates of descent rates from the vortex-averaged quantities would seem to be reasonably realistic.

4 Meteorology

The evolution of the temperature and zonal winds during the major warming is described in detail in Manney et al. (2009b). To further understand the temporal evolution of the stratosphere before, during and after the major warming, we consider Northern Hemisphere (NH) ECMWF 2-D analysed fields of geopotential height at 1200 UTC for four dates spanning the period of the major warming: 8 January, 20 January, 24 January and 1 February (see Fig. 2). We focus on geopotential height fields at 100 hPa (lower stratosphere; right column, Fig. 3), 10 hPa (mid stratosphere; middle column, Fig. 3) and 1 hPa (upper stratosphere; left column, Fig. 3).

MLS orbits are chosen to cut through the cyclonic and anticyclonic circulations present during the period of the major warming. These orbits are used in Sect. 5.2 to produce the line plots (1-D along orbit picture) comparing water vapour analyses and observations, and PV analyses, at various theta levels spanning the stratosphere (Figs. 5–7; right columns). These orbits are also indicated in the left and middle columns of Figs. 5–7, superimposed on the 2-D water vapour analysed fields and PV fields, respectively. The starting point of the MLS orbits indicated in Fig. 3 is labelled

The 2009 stratospheric major warming

W. A. Lahoz et al.

Title Page

Abstract

Introduction

Conclusions

References

Tables

Figures

◀

▶

◀

▶

Back

Close

Full Screen / Esc

Printer-friendly Version

Interactive Discussion



with a closed circle. The temporal evolution of the geopotential height fields during the period 8 January–1 February 2009 is described below. Manney et al. (2009b) provides details of the evolution of the geopotential height fields for the period December 2008–March 2009 (see their Fig. 1).

5 On 8 January (Fig. 3, top row), the cyclonic polar vortex extends throughout the stratosphere from 100 hPa to 1 hPa, with a westward tilt with height. It is roughly axisymmetric, especially at 10 hPa. At 10 hPa and 1 hPa there is an anticyclone over Eastern Siberia. By 16 January (not shown), the polar vortex has become elongated throughout the stratosphere, with a rough orientation of 90°W – 90°E . At 100 hPa and
10 10 hPa the polar vortex is composed of two cyclonic circulations, these being more distinctive at 100 hPa. At 100 hPa there is a ridge of high pressure over the North Pacific pushing into the polar vortex. At 10 hPa and 1 hPa there are two anticyclones, one over the North Pacific, the other over the Bay of Biscay. These anticyclones are tilted westward with height, and push into the cyclonic polar vortex, contributing to its
15 elongation.

By 20 January (Fig. 3, second row), the ridge over the North Pacific at 100 hPa has pushed further into the polar vortex, still composed of two cyclonic circulations. The polar vortex now has a rough orientation of 135°W – 45°E . The two anticyclones seen at 10 hPa and 1 hPa on 16 January have strengthened, are now located over North
20 America and Central Siberia, and have moved toward the polar vortex, contributing to its further elongation, and at 1 hPa causing it to split (Manney et al., 2009b, states that the vortex split on ~ 20 January at 1700 K, ~ 2 hPa). At 10 hPa and 1 hPa the geopotential height pattern is of wavenumber-2 (vortex-split) type, and the anticyclones have strength comparable to that of the cyclonic circulations. At this time the polar
25 vortex is severely distorted in the upper stratosphere.

By 24 January (Fig. 3, third row), the date when major warming criteria are met (Manney et al., 2009b), the anticyclone over the North Pacific at 100 hPa is weaker than on 20 January, and the polar vortex has elongated further. At 10 hPa, the anticyclones have moved further toward the North Pole, and split the polar vortex into two circu-

The 2009 stratospheric major warming

W. A. Lahoz et al.

[Title Page](#)[Abstract](#)[Introduction](#)[Conclusions](#)[References](#)[Tables](#)[Figures](#)[⏪](#)[⏩](#)[◀](#)[▶](#)[Back](#)[Close](#)[Full Screen / Esc](#)[Printer-friendly Version](#)[Interactive Discussion](#)

lations located over North America and Central Siberia (Manney et al., 2009b, states that the vortex split on ~ 24 January at 850 K, ~ 10 hPa). The circulation (cyclones and anticyclones) exhibits the wavenumber-2 pattern of a warming of the vortex-split type. At 10 hPa, the anticyclones remain comparable in strength to the cyclonic circulations.

At 1 hPa, there is a strong anticyclone over the North Pole, and the polar vortex has split into three weak circulations located over East Siberia, North West America and the Atlantic. At this time the polar vortex is severely distorted in the mid and upper stratosphere.

By 1 February (Fig. 3, bottom row), there are two distinct cyclonic circulations at 100 hPa, located over North America and Central Siberia, indicating a vortex split (Manney et al., 2009b, states that the vortex split on ~ 30 January at 520 K, ~ 50 hPa); the timings of the vortex split in the upper, mid and lower stratosphere (~ 20 January, ~ 24 January and ~ 30 January, respectively) are consistent with the typical top-down development of major warmings. At 10 hPa the anticyclone is strong and is located over the North Pole; the cyclonic circulations, located over North West America, Central Siberia and South West Europe, have weakened (and are weaker than the anticyclone). At 1 hPa the circulation is dominated by a broad but weak cyclonic system with two circulations, located over Northern Canada and Central Siberia. At high latitudes, there is no longer a signature of an anticyclone at 1 hPa. At this time the polar vortex has recovered in the upper stratosphere, but is severely distorted in the lower and mid stratosphere.

By 15 February (not shown), at 100 hPa there is a broad cyclonic circulation over Eastern Siberia, with a weaker anticyclonic circulation over Hudson Bay. No significant recovery of the lower stratospheric vortex occurred after the major warming (Manney et al., 2009b). At 10 hPa there are very weak cyclonic and anticyclonic circulations, while at 1 hPa the axi-symmetric cyclonic circulation found over the North Pole in early February is still present. At this time the vortex has strengthened in the upper stratosphere and remains severely distorted in the lower and mid stratosphere. Zonal mean zonal winds remained westerly in the upper mesosphere (~ 90 km) until mid March and

The 2009 stratospheric major warming

W. A. Lahoz et al.

Title Page

Abstract

Introduction

Conclusions

References

Tables

Figures

◀

▶

◀

▶

Back

Close

Full Screen / Esc

Printer-friendly Version

Interactive Discussion



in the lower mesosphere (~ 75 km) until the end of March (see Fig. 1 in Manney et al., 2009b).

5 Evolution of water vapour analyses and PV fields

5.1 Data assimilation versus gridding picture

5 We illustrate the added value of data assimilation with respect to gridded observations. This provides information on the benefit provided by data assimilation. To do this, we compare for one of the selected dates in Sect. 4 BASCOE water vapour analyses with analogous fields of gridded MLS water vapour observations at 850 K (~ 10 hPa) (Fig. 4). The MLS data are linearly gridded onto the latitude-longitude grid $2^\circ \times 5^\circ$ as in Manney et al. (2007) – see their Fig. 4. The BASCOE analyses are shown for five time-stamps
10 (00:00, 06:00, 12:00, 18:00 and 24:00 UTC) at the selected dates; the gridded MLS data are a 24-h average at the selected dates.

Figure 4 shows the BASCOE water vapour analyses (panels 1–5) and gridded MLS water vapour observations (panel 6) at 850 K for 24 January. This shows that at the time
15 of the major warming both the gridded data and analyses show the same broad-scale features; however, the analyses are more fluid-like than the gridded data, suggesting that the former are more physically realistic than the latter. In particular, the analyses do not have the signature of the orbits and other noisy features seen in the gridded data. Because the gridding of the MLS data does not take account of observational
20 error, noisy features in the data are retained in Fig. 4 (panel 6). The spatial relationship between dynamical features (e.g. cyclonic and anticyclonic circulations, identified by relatively high and relatively low water vapour values, respectively) is more realistic, and becomes clearer in the analyses. Figure 4 also shows that the BASCOE water vapour analyses capture well the temporal evolution of the water vapour field. A
25 comparison of the BASCOE analyses and the gridded MLS observations for 8 and 20 January and 1 February (not shown) confirms the conclusions inferred from Fig. 4.

The 2009 stratospheric major warming

W. A. Lahoz et al.

Title Page

Abstract

Introduction

Conclusions

References

Tables

Figures



Back

Close

Full Screen / Esc

Printer-friendly Version

Interactive Discussion



Figure 4 illustrates how data assimilation adds value to the MLS water vapour gridded observations in both space and time. This added value comes from the intelligent interpolation in space and time afforded by the model (the BASCOE CTM) incorporated in the data assimilation method (see discussion in Lahoz et al., 2010).

5.2 Combined 2-D maps/1-D along-orbit picture

We use a combined 2-D maps/1-D along-orbit picture to study the period of the major warming using information from water vapour analyses and PV fields. To do this we present in Figs. 5–7, for selected dates (8, 20, 24 January; 1 February) and theta levels (550 K, 850 K, 1700 K), the BASCOE water vapour analyses (left columns, Figs. 5–7) and the ECMWF PV fields (middle columns, Figs. 5–7). Figs. 5–7 (right columns) show the BASCOE analyses and PV fields, as well as the MLS water vapour observations, linearly interpolated to the orbit indicated (left/middle columns, Figs. 5–7), which marks the horizontal location of MLS water vapour observations. Using PV fields derived from GEOS-5 (Manney et al., 2007; <http://mls.jpl.nasa.gov/dmp>) shows no significant differences in the results (not shown).

Figure 5 concerns the 550 K level (~ 40 hPa, lower stratosphere); Fig. 6 the 850 K level (~ 10 hPa, mid stratosphere); and Fig. 7 the 1700 K level (~ 2 hPa, upper stratosphere). The ECMWF PV fields shown in Figs. 5–7 are calculated using ECMWF vorticity and temperature at a horizontal resolution of $1^\circ \times 1^\circ$, and at 12:00 UTC. PV maps are shown at this resolution, which means they are at a higher resolution than the BASCOE analyses. Note that Lahoz et al. (2009) have tested the performance of the ECMWF PV in the upper stratosphere/lower mesosphere (in particular, the performance at the 1900 K level, ~ 0.8 hPa, was evaluated) and find it provides a realistic description of the large-scale dynamics.

During January–February, throughout the lower and mid stratosphere, the cyclonic circulations in the geopotential height fields are reflected in relatively high values in the water vapour analyses and ECMWF PV fields; the anticyclonic circulations in the geopotential height fields are reflected in relatively low values in the water vapour anal-

The 2009 stratospheric major warming

W. A. Lahoz et al.

Title Page

Abstract

Introduction

Conclusions

References

Tables

Figures

◀

▶

◀

▶

Back

Close

Full Screen / Esc

Printer-friendly Version

Interactive Discussion



yses and PV fields. By contrast, in the upper stratosphere until late January (~28 January), the relationship between the geopotential height and PV fields is opposite, with cyclonic circulations in the geopotential height fields reflected in relatively low values in the water vapour analyses, and the anticyclonic circulations in the geopotential height fields reflected in relatively high values in the water vapour analyses. After late January, this relationship is reversed, and is the same as that seen in the mid and lower stratosphere.

The temporal evolution and spatial distribution of the water vapour analyses and ECMWF PV fields described above is consistent with the strong diabatic descent typical of the Arctic autumn and early winter (e.g., Manney et al., 1994) and shown in other MLS trace gases during the 2005, 2006 and 2009 winters by Manney et al. (2007, 2009a, b), with descent during January bringing down relatively dry mesospheric air at high latitudes to the upper and mid stratosphere (where the ambient air is relatively moist), in regions identified by higher PV values, i.e., the polar vortex. By late January after major warming criteria are met on 24 January, the dry mesospheric air has not yet descended to the mid stratosphere. At this time, the vortex remains sufficiently intact in the mid stratosphere to continue to confine most of the relatively moist air in it. After late January, as the relatively dry air mixes with the ambient moister air, the water vapour mixing ratios throughout the upper and mid stratosphere increase, reflecting the larger extent of the ambient air mass. This has the effect of changing the relationship at 1700 K between the relative moistness/dryness of the air masses and the relative magnitude of the PV associated with them: during January, relatively dry/moist air masses have relatively high/low PV, respectively; during February, relatively moist/dry air masses have relatively high/low PV, respectively. Although PV/tracer correlations can break down in the upper stratosphere/lower mesosphere, as shown here and noted by various authors (Feist et al., 2007; Lahoz et al., 2009; Harvey et al., 2009), these are usually robust at the isentropic levels shown in this paper (see Harvey et al., 2009).

The 2009 stratospheric major warming

W. A. Lahoz et al.

[Title Page](#)[Abstract](#)[Introduction](#)[Conclusions](#)[References](#)[Tables](#)[Figures](#)[◀](#)[▶](#)[◀](#)[▶](#)[Back](#)[Close](#)[Full Screen / Esc](#)[Printer-friendly Version](#)[Interactive Discussion](#)

The 2009 stratospheric major warming

W. A. Lahoz et al.

[Title Page](#)[Abstract](#)[Introduction](#)[Conclusions](#)[References](#)[Tables](#)[Figures](#)[⏪](#)[⏩](#)[◀](#)[▶](#)[Back](#)[Close](#)[Full Screen / Esc](#)[Printer-friendly Version](#)[Interactive Discussion](#)

Comparison of the fields at 550 K (Fig. 5) shows that, qualitatively, the water vapour analyses and water vapour observations track the PV values, with relatively low values at low and mid NH latitudes and high values at high NH latitudes on 8 January, when the polar vortex in the lower stratosphere is not very distorted and is centred roughly over the North Pole. This is confirmed in the agreement between the location of the cyclonic circulation in Fig. 3 (top row), the vortex identified by relatively high PV values in Fig. 5 (top row, middle column), and the along-orbit cuts (Fig. 5, top row, right column, profiles 2425–2465, latitudes poleward of $\sim 55^\circ$ N).

As the vortex elongates over the period 20–24 January, the water vapour fields continue to track the evolving PV field, with relatively high/low values in the former corresponding to relatively high/low values in the latter. This is confirmed in the agreement between the water vapour and PV analyses, and the along-orbit cuts in Fig. 5: second row, right column (profiles 2740–2780, latitudes from $\sim 70^\circ$ N ascending node to $\sim 55^\circ$ N descending node); and third row, right column (profiles 980–1025, latitudes poleward of $\sim 50^\circ$ N). The ascending node is between the start of the orbit and the northernmost latitude on the orbit track; the descending node is between the northernmost latitude on the orbit track and the end of the orbit.

By 1 February, when the vortex has split into two, the split is seen in both the water vapour and the PV field, with relatively high values in both fields corresponding to cyclonic circulations, and relatively low values in both fields corresponding to air in between cyclonic circulations. As before, this is confirmed in the agreement between the water vapour and PV analyses, and the along-orbit cuts in Fig. 5, fourth row, right column (profiles 1335–1350 and 1380–1395, latitudes $\sim 40^\circ$ N– 60° N ascending node, latitudes $\sim 70^\circ$ N– 50° N descending node).

Inspection of the water vapour and PV along-orbit plots at 850 K (Fig. 6) shows that, qualitatively, the water vapour analyses and water vapour observations also track the evolving PV field during the period of the major warming. This is confirmed in the agreement between the cyclonic circulations in Fig. 3, and the vortex features identified by relatively high PV values and relatively high water vapour values in Fig. 6, right

column: (i) top row, 8 January, profiles 2425–2460, latitudes from $\sim 55^\circ$ N ascending node to $\sim 60^\circ$ N descending node; (ii) second row, 20 January, profiles 2715–2745 and 2755–2775, latitudes from $\sim 50^\circ$ N to $\sim 70^\circ$ N ascending node, and $\sim 75^\circ$ N to $\sim 45^\circ$ N descending node; (iii) third row, 24 January, profiles 975–995 and 1015–1035, latitudes from $\sim 40^\circ$ N to $\sim 70^\circ$ N ascending node, and $\sim 80^\circ$ N to $\sim 45^\circ$ N descending node; and (iv) bottom row, 1 February, profiles 1340–1350 and 1390–1405, latitudes from $\sim 40^\circ$ N to $\sim 60^\circ$ N ascending node, and $\sim 55^\circ$ N to $\sim 35^\circ$ N descending node. The PV maps on 8 January at 850 K (and 1700 K; see below) show pockets of relatively low PV inside the vortex, an example that PV and tracers may not both increase monotonically into the polar vortex.

Inspection of the water vapour and PV line plots at 1700 K (Fig. 7) shows that, qualitatively, the water vapour analyses and water vapour observations also track the evolving PV field during the period of the major warming, but with a reversed relationship between the water vapour data and the PV analyses until the end of January, which can be understood in terms of the confined diabatic descent characteristic of the Arctic vortex in early winter (see discussion above). This is confirmed in the agreement between the cyclonic circulations in Fig. 3, and the vortex features identified by relatively high PV values and relatively low water vapour values for January in Fig. 7, right column: (i) top row, 8 January, profiles 2410–2460, latitudes from $\sim 50^\circ$ N ascending node to $\sim 65^\circ$ N descending node; (ii) second row, 20 January, profiles 2720–2745, latitudes from $\sim 50^\circ$ N to $\sim 80^\circ$ N ascending node; (iii) third row, 24 January, profiles 985–995, latitudes from $\sim 55^\circ$ N to $\sim 70^\circ$ N ascending node. For 1 February, the PV and water vapour fields are no longer anti-correlated in the regions of highest PV values: Fig. 7, right column, bottom row, profiles 1360–1380, and latitudes from $\sim 70^\circ$ N ascending node to $\sim 70^\circ$ N descending node.

Similar consistency between the water vapour analyses and observations and the PV fields is seen for other orbit cuts at 550 K, 850 K and 1700 K.

In Figs. 5–7, the MLS observations are noisy with oscillations within the 1-sigma random error bars (the solid grey lines in Figs. 5–7, right column, show the estimated

The 2009 stratospheric major warming

W. A. Lahoz et al.

Title Page

Abstract

Introduction

Conclusions

References

Tables

Figures

◀

▶

◀

▶

Back

Close

Full Screen / Esc

Printer-friendly Version

Interactive Discussion



precision of the MLS water vapour observations). The BASCOE analyses and PV fields are comparably smoother than the observations. At the large-scale, all three fields agree well, whereas at the small-scale, the BASCOE analyses agree better with the PV fields. The reason the BASCOE water vapour analyses and PV fields are smoother than the water vapour measurements is likely owing to the assimilation that, by its nature, smoothes the observations, and the relatively higher horizontal resolution of the PV fields.

5.3 Equivalent latitude-theta picture

We use the equivalent latitude-theta picture to look at the water vapour fields for the dates considered in Sects. 3–4 (8, 20, 24 January; 1 February; respectively, left, middle left, middle right and right columns in Fig. 8). We compare the BASCOE water vapour analyses (top row, Fig. 8) with two BASCOE CTM free runs (i.e., without data assimilation): one includes chemistry (middle row, Fig. 8); the other excludes chemistry (bottom row, Fig. 8).

The equivalent latitude-theta maps for the BASCOE analyses (top row, Fig. 8) show several notable features. First, they show relatively dry air (mixing ratios less than 6 ppmv) in the mesosphere (theta values greater than ~ 2100 K) poleward of 50° N on 8 January, identified to be mainly within the polar vortex in terms of geopotential height (Fig. 3), or of water vapour or PV (Fig. 7). By 20 January, this air mass has descended to ~ 1500 K and by 24 January to ~ 1300 K, mainly remaining within the polar vortex (see left column, second and third row; Fig. 3). By 1 February, no mixing ratios lower than 6 ppmv can be seen poleward of 50° N and theta levels higher than ~ 1200 K, suggesting that these air masses of mesospheric origin have mixed in with the relatively moist ambient air at these levels (see discussion in Sect. 5.2). This is consistent with the relatively weak latitudinal gradients in the polar vortex on 1 February at 1 hPa (left column, bottom row; Fig. 3). These results suggest a descent of ~ 600 K between 8 January and 20 January (descent rate of ~ 50 K day $^{-1}$), and a descent of ~ 200 K between 20 January and 24 January (descent rate of ~ 50 K day $^{-1}$ also). In Sect. 3 we

The 2009 stratospheric major warming

W. A. Lahoz et al.

Title Page

Abstract

Introduction

Conclusions

References

Tables

Figures



Back

Close

Full Screen / Esc

Printer-friendly Version

Interactive Discussion



estimated descent rates for this relatively dry air of between 40 K day^{-1} and 60 K day^{-1} .

Second, the equivalent latitude-theta maps show an air mass of relatively moist air (mixing ratios greater than 6.5 ppmv) in the mid stratosphere ($\sim 600 \text{ K}$ – $\sim 1000 \text{ K}$) poleward of 50° N at 1700 K on 8 January, identified to be within the polar vortex in terms of geopotential height (Fig. 3), or of water vapour or PV (Fig. 6). This air mass remains coherent over the rest of January, although decreasing in extent both in the vertical and the horizontal, with its upper layers descending to $\sim 850 \text{ K}$ by 20 January (descent rate of $\sim 10 \text{ K day}^{-1}$) and to $\sim 750 \text{ K}$ by 1 February (descent rate of 10 K day^{-1} also). The lower layers of this air mass remain at $\sim 650 \text{ K}$ during this period (8 January–1 February). In Sect. 3 we estimated descent rates for this relatively moist air of $\sim 5 \text{ K day}^{-1}$.

Third, the equivalent latitude-theta maps show poleward transport of relatively moist air (mixing ratios greater than 6.5 ppmv) at theta levels higher than $\sim 1300 \text{ K}$ between 8 January and 1 February. At $\sim 1300 \text{ K}$, the region of relatively moist air (located equatorward of 50° N on 8 January) decreases in size during this period, and by 1 February only remnants exist. The part of this air mass located at $\sim 1700 \text{ K}$ descends from $\sim 1700 \text{ K}$ (24 January) to $\sim 1600 \text{ K}$ (1 February), a descent rate of $\sim 10 \text{ K day}^{-1}$. Figure 7 confirms the presence of a coherent relatively moist air mass equatorward of 50° N at 1700 K on 8 January.

The CTM runs show little difference between including or excluding chemistry (middle and bottom row, respectively; Fig. 8), confirming that advection and not chemistry is the dominant process affecting the water vapour distribution during the period of the stratospheric major warming (see Sect. 3). The CTM runs capture the large-scale features of the BASCOE analyses (e.g. general location of maxima/minima in the water vapour distribution), but are unable to capture localized features in the analyses, e.g., the relatively moist air in the mid stratosphere ($\sim 850 \text{ K}$) seen on 24 January and 1 February, and the pockets of relatively dry air seen at $\sim 1500 \text{ K}$ on 20 and 24 January poleward of 60° N . As localized features seen in the equivalent latitude-theta representation of the BASCOE analyses are consistent with the meteorological data (see Figs. 3, 6 and 7, and Manney et al., 2009b), this illustrates how data assimilation adds

The 2009 stratospheric major warming

W. A. Lahoz et al.

Title Page

Abstract

Introduction

Conclusions

References

Tables

Figures

◀

▶

◀

▶

Back

Close

Full Screen / Esc

Printer-friendly Version

Interactive Discussion



value to the BASCOE CTM by incorporating information from the MLS observations. A similar conclusion was inferred on the basis of vortex-averaged quantities (Sect. 3).

6 Discussion

We now establish the links between the information provided by Sects. 3–5 above and how this information provides an overall picture of the major warming. Section 3 provides an overview of the wintertime evolution of the stratosphere/lower mesosphere from the point of view of the BASCOE water vapour analyses. Sections 4–5 focus on selected dates during this period. Section 4 identifies the evolution of the meteorology (epitomized by geopotential height fields), emphasizing the central role of the cyclonic polar vortex and its interaction with subsidiary anticyclones. Section 5 illustrates various dynamical aspects of the wintertime evolution, and the added value of data assimilation with respect to the model and observations. We now discuss Sect. 5 in more detail.

Section 5.1 illustrates the added value of data assimilation with respect to observations, with reference to the period of the major warming. Section 5.2 describes the evolution of the stratosphere and lower mesosphere during the major warming using a 1-D along-orbit picture and a 2-D picture (latitude-longitude maps of water vapour analyses and PV). In the 1-D picture, we select orbits that cut through the cyclonic and anticyclonic circulations. These pictures show the dynamical consistency in the evolution of the water vapour (observations and analyses) and PV fields on selected isentropic levels spanning the stratosphere and lower mesosphere. This section also describes how the water vapour field is transported isentropically (i.e., quasi-horizontally) and how the behaviour of the water vapour and PV fields (both tracers) is related to the behaviour of the geopotential height field. This section establishes a clear link between the distribution of the water vapour tracer field and the location and evolution of the polar vortex. Section 5.3 uses the 2-D equivalent latitude-theta picture to provide information on isentropic and vertical transport in the stratosphere and lower mesosphere,

The 2009 stratospheric major warming

W. A. Lahoz et al.

Title Page

Abstract

Introduction

Conclusions

References

Tables

Figures



Back

Close

Full Screen / Esc

Printer-friendly Version

Interactive Discussion



and illustrate the added value of data assimilation with respect the BASCOE CTM, with reference to the period of the major warming.

Descent rates of various air masses during the major warming are estimated from BASCOE analyses using an equivalent latitude-theta approach (Sect. 5.3) and a vortex-averaged approach (Sect. 3); they are shown to be consistent with each other. These estimates are compared with estimates based on Fig. 2 in Manney et al. (2009b). Estimates using BASCOE analyses are consistent with those based on the material in Manney et al. (2009b), once consideration is taken of the fact that different tracers are being used, and that these tracers have different horizontal gradients.

Descent rates in the wintertime mesosphere and upper stratosphere have been estimated using a number of methods (Lee et al., 2010, and references therein). Lee et al. estimate a descent rate for northern winters 2006 and 2009 (winters with major warmings) of $\sim 0.5 \text{ km day}^{-1}$ at 60 km, comparable to our value of $\sim 1 \text{ km day}^{-1}$ estimated for the region between 50 km and 35 km (Sects. 3, 5.3). Note, however, that as Lee et al. discuss, caution must be used in interpreting their results, as chemical and/or dynamical processes not directly related to descent may affect the method they use to estimate descent rates (namely, changes in the maximum of the CO northern and southern annular mode indices).

7 Conclusions

In this paper we study the evolution of the record-breaking major stratospheric warming of northern winter 2009 (January-February) from synergistic use of MLS water vapour measurements and BASCOE water vapour analyses. These data are supplemented with meteorological data from ECMWF and PV derived from ECMWF meteorological data. We use a 2-D picture (latitude-longitude maps, equivalent latitude-theta maps) to represent the water vapour analyses and PV fields, and a 1-D along-orbit picture to represent the water vapour analyses, PV fields and MLS water vapour measurements.

The 2009 stratospheric major warming

W. A. Lahoz et al.

Title Page

Abstract

Introduction

Conclusions

References

Tables

Figures

◀

▶

◀

▶

Back

Close

Full Screen / Esc

Printer-friendly Version

Interactive Discussion



The 2009 stratospheric major warming

W. A. Lahoz et al.

Title Page

Abstract

Introduction

Conclusions

References

Tables

Figures

◀

▶

◀

▶

Back

Close

Full Screen / Esc

Printer-friendly Version

Interactive Discussion



By combining the information from the 1-D and 2-D pictures we obtain a comprehensive, consistent and physically realistic 3-D picture of the stratosphere during the period of the major warming. This focuses on the interaction between the cyclonic wintertime stratospheric polar vortex and subsidiary anticyclonic stratospheric circulations prevalent during this period.

This study provides evidence of the benefit of using stratospheric water vapour analyses (produced using data assimilation), together with water vapour observations, meteorological data and PV fields, to help understand the 3-D dynamical evolution of the stratosphere during an interesting dynamical event such as a major stratospheric warming. Data assimilation fills in the observational gaps objectively, and allows computation of vortex-averaged quantities to provide a realistic picture of the descent of tracer isopleths in the stratosphere. Estimates of descent rates in the polar vortex appear to be realistic and consistent with those estimated from Manney et al. (2009b). The benefits of assimilating MLS satellite data into the BASCOE model are demonstrated: namely, a more realistic spatial and temporal representation of the water vapour field.

Future work will aim to test further the benefits of the approach used in this paper by applying it to study other interesting stratospheric dynamical and events, including the final warming in the northern and southern winter stratosphere.

Acknowledgements. Thanks to the MLS team and the EOS Aura project for their roles in producing, documenting and distributing the MLS data. Thanks to William Daffer (Jet Propulsion Laboratory) for data analysis/graphics assistance. The WAVACS COST Action funded a Short Term Scientific Mission (STSM) for S. Viscardy to visit NILU. WAL is supported by an internal NILU project and by RTRA/STAE during his time at CNRM-GAME. QE and SV are supported by the Belgian Federal Science Policy in the framework of the SECPEA ProDEX project. Work at the Jet Propulsion Laboratory, California Institute of Technology was done under contract with the National Aeronautics and Space Administration. Thanks to Finn Bjørklid (NILU) for improving the layout of various figures.

The publication of this article is financed by CNRS-INSU.

References

- Baldwin, M. P. and Dunkerton, T. J.: Stratospheric harbingers of anomalous weather regimes, *Science*, 294, 581–584, 2001.
- Bernath, P. F., McElroy, C. T., Abrams, M. C., et al.: Atmospheric Chemistry Experiment (ACE): Mission overview, *Geophys. Res. Lett.*, 32, L15S01, doi: 10.1029/2005GL022386, 2005.
- Charlton, A. J. and Polvani, L. M.: A New Look at Stratospheric Sudden Warmings. Part I: Climatology and Modeling Benchmarks, *J. Climate*, 20, 449–469, doi:10.1175/JCLI3996.1, 2007.
- Charlton-Perez, A. J., Polvani, L. M., Austin, J. and Li, F.: The frequency and dynamics of stratospheric sudden warmings in the 21st century, *J. Geophys. Res.*, 113, D16116, doi:10.1029/2007JD009571, 2008.
- El Amraoui, L., Semane, N., Peuch, V.-H. and Santee, M. L.: Investigation of dynamical processes in the polar stratospheric vortex during the unusually cold winter 2004/2005, *Geophys. Res. Lett.*, 35, L03803, doi:10.1029/2007GL031251, 2008.
- Errera, Q., Daerden, F., Chabrillat, S., et al.: 4D-Var assimilation of MIPAS chemical observations: Ozone and nitrogen dioxide analyses, *Atmos. Chem. Phys.*, 8, 6169–6187, doi:10.5194/acp-8-6169-2008, 2008.
- Errera, Q. and Fonteyn, D.: Four-dimensional variational chemical data assimilation of CRISTA stratospheric measurements, *J. Geophys. Res.*, 106, 12253–12265, 2001.
- Feist, D.G., Geer, A.J., Müller, S. and Kämpfer, N.: Middle atmosphere water vapour and dynamical features in aircraft measurements and ECMWF analyses. *Atmos. Chem. Phys.*, 7, 5291–5307, doi:10.5194/acp-7-5291-2007, 2007.
- Geer, A. J., Lahoz, W. A., Bekki, S., et al.: The ASSET intercomparison of ozone analyses:

The 2009 stratospheric major warming

W. A. Lahoz et al.

Title Page

Abstract

Introduction

Conclusions

References

Tables

Figures

⏪

⏩

◀

▶

Back

Close

Full Screen / Esc

Printer-friendly Version

Interactive Discussion



**The 2009
stratospheric major
warming**

W. A. Lahoz et al.

[Title Page](#)[Abstract](#)[Introduction](#)[Conclusions](#)[References](#)[Tables](#)[Figures](#)[◀](#)[▶](#)[◀](#)[▶](#)[Back](#)[Close](#)[Full Screen / Esc](#)[Printer-friendly Version](#)[Interactive Discussion](#)

method and first results, *Atmos. Chem. Phys.*, 6, 5445–5474, doi:10.5194/acp-6-5445-2006, 2006.

5 Geer, A. J., Lahoz, W. A., Jackson, D. R., et al.: Evaluation of linear photochemistry parametrizations in a stratosphere-troposphere data assimilation system, *Atmos. Chem. Phys.*, 7, 939–959, doi:10.5194/acp-7-939-2007, 2007.

Harvey, V. L., Pierce, R. B., Fairlie, T. D. and Hitchman, M. H.: A climatology of stratospheric polar vortices and anticyclones, *J. Geophys. Res.*, 107, 4442, doi:10.10129/2001JD001471, 2002.

10 Harvey, V. L., Pierce, R. B., Hitchman, M. H., Randall, C. E. and Fairlie, T. D.: On the distribution of ozone in stratospheric anticyclones, *J. Geophys. Res.*, 109, D24308, doi:10.1029/2004JD00004992, 2004.

Harvey, V. L., Randall, C. E. and Hitchman, M. H.: Breakdown of potential vorticity-based equivalent latitude as vortex-centered coordinate in the polar winter mesosphere. *J. Geophys. Res.*, 114, D22105, doi:10.10129/2009JD012681, 2009.

15 Jackson, D. R. and Orsolini, Y. J.: Estimation of Arctic ozone loss in winter 2004/2005 based on assimilation of EOS MLS and SBUV/2 observations, *Q. J. Roy. Meteor. Soc.*, 134, 1833–1841, 2008.

Labitzke, K. and Kunze, M.: On the remarkable Arctic winter in 2008/2009, *J. Geophys. Res.*, 114, D00102, doi:10.1029/2009JD012273, 2009.

20 Lahoz, W. A., Errera, Q., Swinbank, R., and Fonteyn, D.: Data assimilation of stratospheric constituents: A review, *Atmos. Chem. Phys.*, 7, 5745–5773, doi:10.5194/acp-7-5745-2007, 2007a.

Lahoz, W. A., Geer, A. J., Bekki, S., et al.: The Assimilation of Envisat data (ASSET) project, *Atmos. Chem. Phys.*, 7, 1773–1796, doi:10.5194/acp-7-1773-2007, 2007b.

25 Lahoz W.A., Geer, A.J. and O'Neill, A.: Dynamical evolution of the 2003 Southern Hemisphere stratospheric winter using Envisat trace gas observations, *Q. J. Roy. Meteorol. Soc.*, 132, 1985–2008, 2006.

Lahoz, W. A., Khattatov, B., and Ménard, R.: Data Assimilation and Information, in *Data Assimilation: Making Sense of Observations*, edited by: Lahoz, W. A., Khattatov, B., and Ménard, R., Springer, 3–12, 2010.

30 Lahoz, W. A., O'Neill, A., Carr, E. S., et al.: Three-dimensional evolution of water vapor distributions in the Northern Hemisphere stratosphere as observed by the MLS, *J. Atmos. Sci.*, 51, 2914–2930, 1994.

**The 2009
stratospheric major
warming**W. A. Lahoz et al.

[Title Page](#)[Abstract](#)[Introduction](#)[Conclusions](#)[References](#)[Tables](#)[Figures](#)[◀](#)[▶](#)[◀](#)[▶](#)[Back](#)[Close](#)[Full Screen / Esc](#)[Printer-friendly Version](#)[Interactive Discussion](#)

Lahoz, W. A., O'Neill, A., Heaps, A., et al.: Vortex dynamics and the evolution of water vapour in the stratosphere of the Southern Hemisphere, *Q. J. Roy. Meteorol. Soc.*, 122, 423–450, 1996.

Lahoz, W. A., Orsolini, Y. J., Geer, A. J., Choi, W. and Allen, D.: Mesosphere-stratosphere transport during southern hemisphere autumn deduced from MIPAS observations, *Q. J. Roy. Meteorol. Soc.*, 135, 681–694, 2009.

Lambert, A., Read, W. G., Livesey, N. J., et al.: Validation of the Aura Microwave Limb Sounder middle atmosphere water vapor and nitrous oxide measurements, *J. Geophys. Res.*, 112, D24S36, doi:10.1029/2007JD008724, 2007.

Lee, J. N., Wu, D. L., Manney, G. L., et al.: Aura Microwave Limb Sounder Observations of the Polar Middle Atmosphere: Dynamics and transport of CO and H₂O, *J. Geophys. Res.*, submitted, 2010.

Livesey, N. J., Read, W. G., Lambert, A., et al.: Earth Observing System (EOS) Aura Microwave Limb Sounder (MLS) Version 2.2 Level 2 data quality and description document, JPL D-33509, Jet Propulsion Laboratory, California Institute of Technology, Pasadena, California, available online at: http://mls.jpl.nasa.gov/v2-2_data_quality_document.pdf, 91109-8099, 2007.

Manney, G. L., Daffer, W. H., Zawodny, J. M., et al.: Solar occultation satellite data and derived meteorological products: Sampling issues and comparisons with Aura Microwave Limb Sounder, *J. Geophys. Res.*, 112, D24S50, doi:10.1029/2007JD008709, 2007.

Manney, G. L., Harwood, R. S., Mackenzie, I. A., et al.: Satellite observations and modelling of transport in the upper troposphere through the lower mesosphere during the 2006 major stratospheric sudden warming, *Atmos. Chem. Phys.*, 9, 4775–4795, doi:10.5194/acp-9-4775-2009, 2009a.

Manney, G. L., Krüger, K., Pawson, S., et al.: The evolution of the stratopause during the 2006 major warming: Satellite data and assimilated meteorological analyses, *J. Geophys. Res.*, 113, D11115, doi:10.1029/2007JD009097, 2008.

Manney, G. L., Santee, M. L., Livesey, N. J., et al.: EOS Microwave Limb Sounder observations of the Antarctic polar vortex breakup in 2004, *Geophys. Res. Lett.*, 32, L12811, doi:10.1029/2005GL022823, 2005.

Manney, G. L., Schwartz, M. J., Krüger, K., et al.: Aura Microwave Limb Sounder Observations of Dynamics and Transport During the Record-breaking 2009 Arctic Stratospheric Major Warming, *Geophys. Res. Lett.*, 36, L12815, doi:10.1029/2009GL038586, 2009b.

**The 2009
stratospheric major
warming**W. A. Lahoz et al.

[Title Page](#)[Abstract](#)[Introduction](#)[Conclusions](#)[References](#)[Tables](#)[Figures](#)[◀](#)[▶](#)[◀](#)[▶](#)[Back](#)[Close](#)[Full Screen / Esc](#)[Printer-friendly Version](#)[Interactive Discussion](#)

Manney, G. L., Zurek, R. W., O'Neill, A., and Swinbank, R.: On the Motion of Air through the Stratospheric Polar Vortex, *J. Atmos. Sci.*, 51, 2973–2994, 1994.

Mechoso, C. R., O'Neill, A., Pope, V. D., and Farrara, J. D.: A study of the stratospheric final warming of 1982 in the southern hemisphere, *Q. J. Roy. Meteor. Soc.*, 114, 1365–1384, 1988.

Pumphrey, H. C., Filipiak, M. J., Livesey, N. J., et al.: Validation of middle-atmosphere carbon monoxide retrievals from the Microwave Limb Sounder on Aura, *J. Geophys. Res.*, 112, D24S38, doi:10.1029/2007JD008723, 2007.

Rösevall, J. D., Murtagh, D. P., Urban, J., et al.: A study of ozone depletion in the 2004/2005 Arctic winter based on data from ODIN/SMR and Aura/MLS, *J. Geophys. Res.*, 113, D13301, doi:10.1029/2007JD009560, 2008.

Simmons, A. J., Hortal, M., Kelly, G., et al.: ECMWF analyses and forecasts of stratospheric winter polar vortex breakup: September 2002 in the Southern Hemisphere and related events, *J. Atmos. Sci.*, 62, 668–689, 2005.

Siskind, D. E., Eckermann, S. D., Coy, L., and McCormack, J. P.: On recent interannual variability of the Arctic winter mesosphere: Implications for tracer descent, *Geophys. Res. Lett.*, 34, L09806, doi:10.1029/2007GL029293, 2007.

Thornton, H., Jackson, D. R., Bekki, S., et al.: The ASSET intercomparison of stratosphere and lower mesosphere humidity analyses, *Atmos. Chem. Phys.*, 9, 995–1016, doi:10.5194/acp-9-995-2009, 2009.

Viscardy, S., Errera, Q., Christophe, Y., Chabrilat, S., and Lambert, J.-C.: Evaluation of ozone analyses from UARS MLS assimilation by BASCOE between 1992 and 1999, *JSTARS*, 10.1109/JSTARS.2010.2040463, 109–202, 2010.

WMO: Scientific Assessment of stratospheric ozone depletion: 2006, UN Environmental Programme, Geneva, Switzerland, 2007.

The 2009 stratospheric major warming

W. A. Lahoz et al.

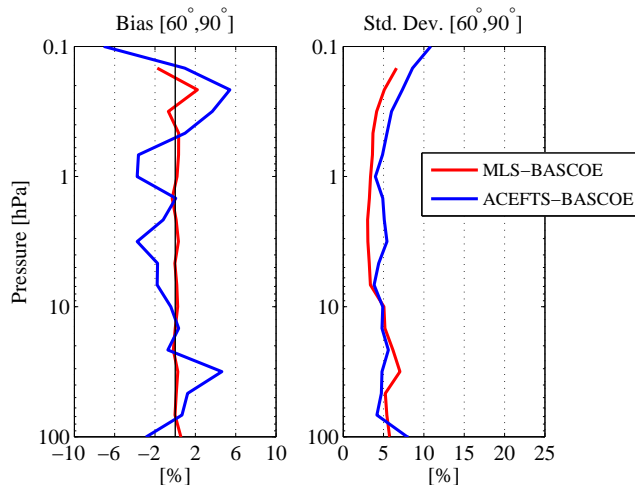


Fig. 1. Bias (left-hand plot) and standard deviation (right-hand plot) of the differences (as a percentage of the observational data) between BASCOE water vapour analyses and MLS water vapour observations (red line), and between BASCOE water vapour analyses and ACE-FTS water vapour observations (blue line), averaged for the period January–February 2009 and over 60° N– 90° N. The x-axis is percent difference (%); the y-axis is pressure (hPa). Positive values in the bias indicate that the BASCOE analyses are moister than the MLS and ACE-FTS data.

[Title Page](#)
[Abstract](#)
[Introduction](#)
[Conclusions](#)
[References](#)
[Tables](#)
[Figures](#)
[⏪](#)
[⏩](#)
[◀](#)
[▶](#)
[Back](#)
[Close](#)
[Full Screen / Esc](#)
[Printer-friendly Version](#)
[Interactive Discussion](#)


The 2009 stratospheric major warming

W. A. Lahoz et al.

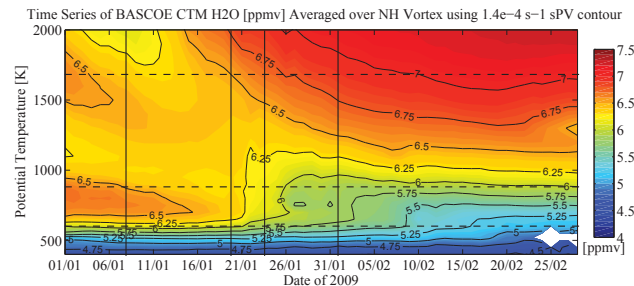
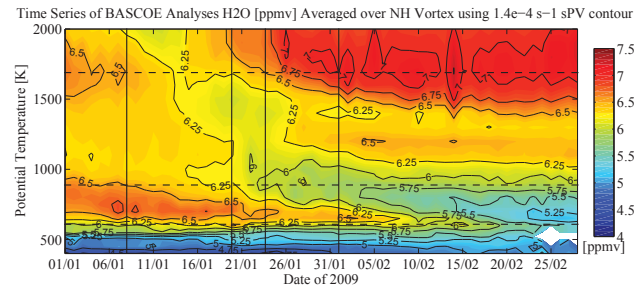


Fig. 2. Times series of NH vortex-averaged water vapour (ppmv) for the period 1 January–28 February 2009 and the theta range 400 K–2000 K. (top) From BASCOE analyses; (bottom) from BASCOE CTM run (no assimilation), with chemistry. Blue-green denotes relatively low values; red denotes relatively high values. The vortex average is computed for PV values identified to be within the polar vortex, the edge of the vortex estimated to be at 1×10^{-4} s⁻¹ for a scaled PV (Manney et al., 2007). The white area indicates where it is not possible to calculate the vortex edge. The vertical black solid lines identify the dates 8 January, 20 January, 24 January and 1 February (left to right). The horizontal black dashed lines identify the theta levels 550 K, 850 K and 1700 K (bottom to top).

Title Page

Abstract

Introduction

Conclusions

References

Tables

Figures

◀

▶

◀

▶

Back

Close

Full Screen / Esc

Printer-friendly Version

Interactive Discussion



The 2009 stratospheric major warming

W. A. Lahoz et al.

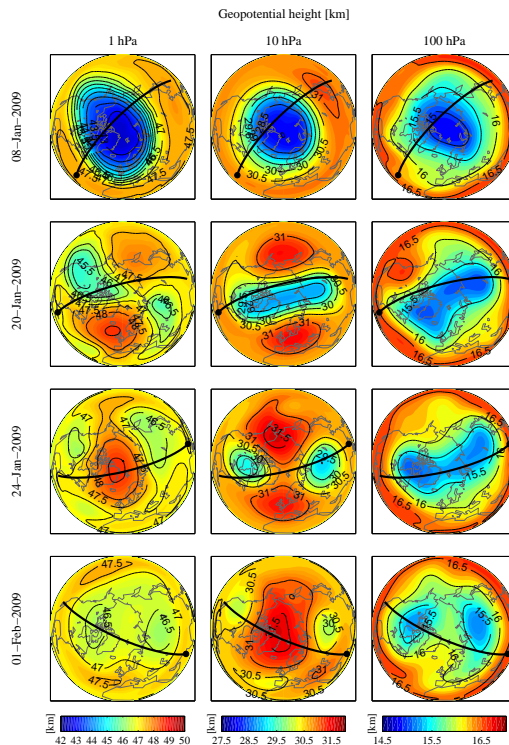


Fig. 3. (Top row) NH ECMWF geopotential height field (km), 12:00 UTC 8 January 2009, at 1 hPa (left column), 10 hPa (middle column) and 100 hPa (right column). Red indicates relatively high geopotential height values (anticyclonic circulation); blue indicates relatively low geopotential height values (cyclonic circulation). The orbit indicated (profiles 2400–2490) is used to produce the plots comparing the analyses, measurements and PV in Figs. 5–7; the starting point is labelled with a closed circle. (Second row) As (Top row) but for 20 January 2009. The orbit indicated (profiles 2700–2790) is used to produce the plots comparing the analyses, measurements and PV in Figs. 5–7; the starting point is labelled with a closed circle. (Third row) As (Top row) but for 24 January 2009. The orbit indicated (profiles 960–1050) is used to produce the plots comparing the analyses, measurements and PV in Figs. 5–7; the starting point is labelled with a closed circle. (Bottom row) As (Top row) but for 1 February 2009. The orbit indicated (profiles 1320–1410) is used to produce the plots comparing the analyses, measurements and PV in Figs. 5–7; the starting point is labelled with a closed circle.

Title Page

Abstract

Introduction

Conclusions

References

Tables

Figures

◀

▶

◀

▶

Back

Close

Full Screen / Esc

Printer-friendly Version

Interactive Discussion



The 2009 stratospheric major warming

W. A. Lahoz et al.

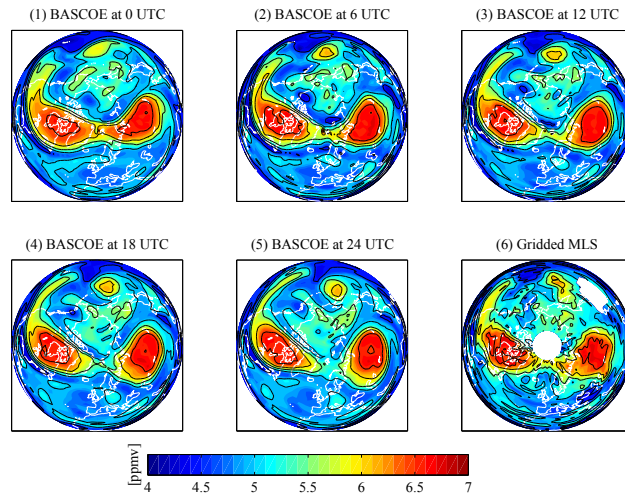


Fig. 4. BASCOE water vapour analyses (ppmv) at 00:00, 06:00, 12:00, 18:00 and 24:00 UTC on 24 January 2009 at 850 K (panels 1–5, respectively); gridded MLS water vapour observations (ppmv; 24-hour average) on 24 January 2009 at 850 K (panel 6). Red indicates relatively high values; blue indicates relatively low values. White areas in panel 6 indicate a lack of observations.

[Title Page](#)[Abstract](#)[Introduction](#)[Conclusions](#)[References](#)[Tables](#)[Figures](#)[◀](#)[▶](#)[◀](#)[▶](#)[Back](#)[Close](#)[Full Screen / Esc](#)[Printer-friendly Version](#)[Interactive Discussion](#)

The 2009 stratospheric major warming

W. A. Lahoz et al.

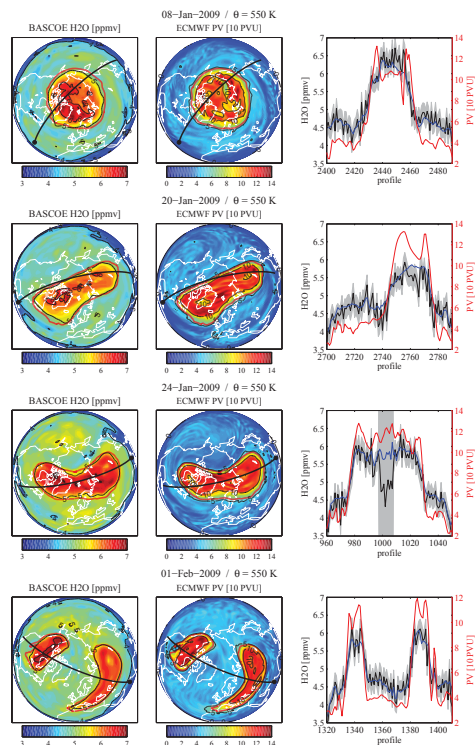


Fig. 5. Plots of geophysical quantities at 550 K. NH BASCOE water vapour analyses (ppmv), left column; NH ECMWF PV field (10×PV units), middle column; MLS water vapour measurements (black line, ppmv), BASCOE water vapour analyses (blue line, ppmv), and ECMWF PV fields (red line, 10×PV units) interpolated to the orbits indicated in left and middle columns, right column. Top row: 8 January 2009; second row: 20 January 2009; third row: 24 January 2009; bottom row: 1 February 2009. In the left and middle columns, red indicates relatively high values; blue indicates relatively low values; bold red contours indicate the vortex edge (see text for definition). In the right column, grey indicates the precision in the MLS water vapour measurements.

Title Page

Abstract

Introduction

Conclusions

References

Tables

Figures

◀

▶

◀

▶

Back

Close

Full Screen / Esc

Printer-friendly Version

Interactive Discussion



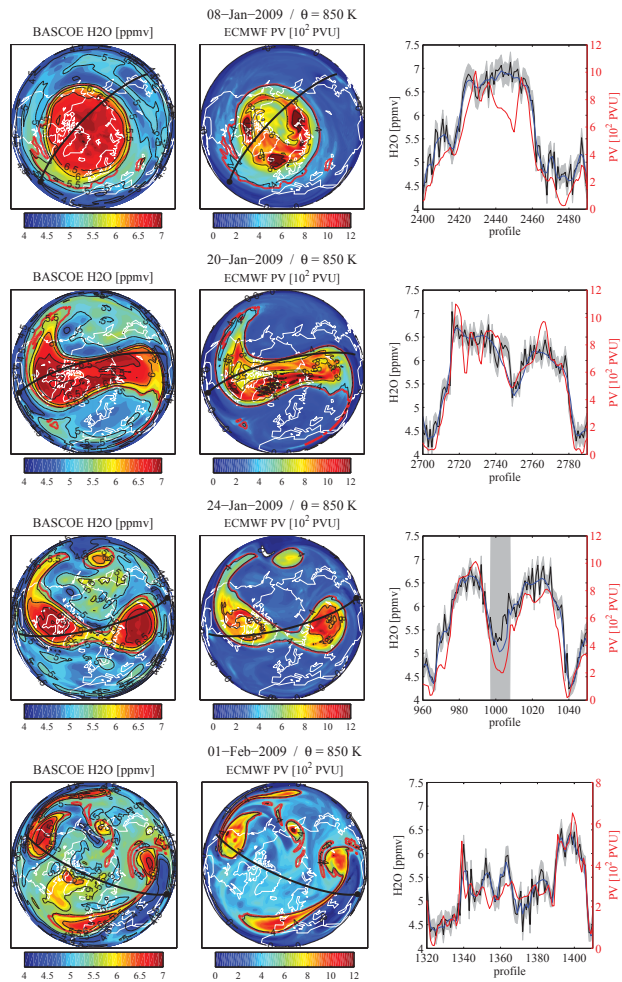


Fig. 6. As Fig. 5 but at 850 K.

The 2009 stratospheric major warming

W. A. Lahoz et al.

Title Page

Abstract Introduction

Conclusions References

Tables Figures

◀ ▶

◀ ▶

Back Close

Full Screen / Esc

Printer-friendly Version

Interactive Discussion



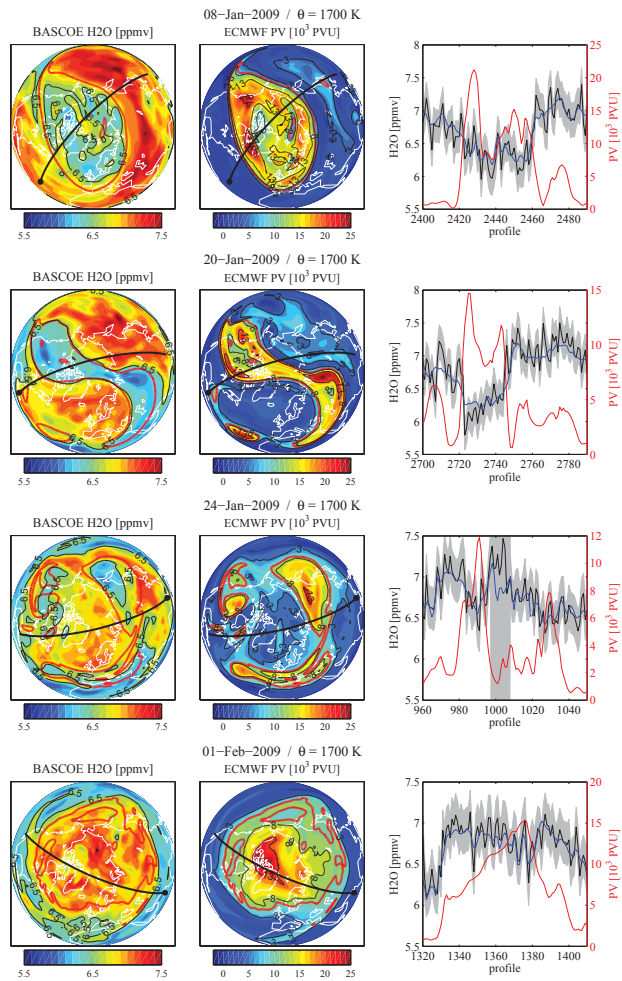


Fig. 7. As Fig. 5 but at 1700 K.

Discussion Paper | Discussion Paper | Discussion Paper | Discussion Paper

The 2009 stratospheric major warming

W. A. Lahoz et al.

Title Page

Abstract Introduction

Conclusions References

Tables Figures

◀ ▶

◀ ▶

Back Close

Full Screen / Esc

Printer-friendly Version

Interactive Discussion



The 2009 stratospheric major warming

W. A. Lahoz et al.

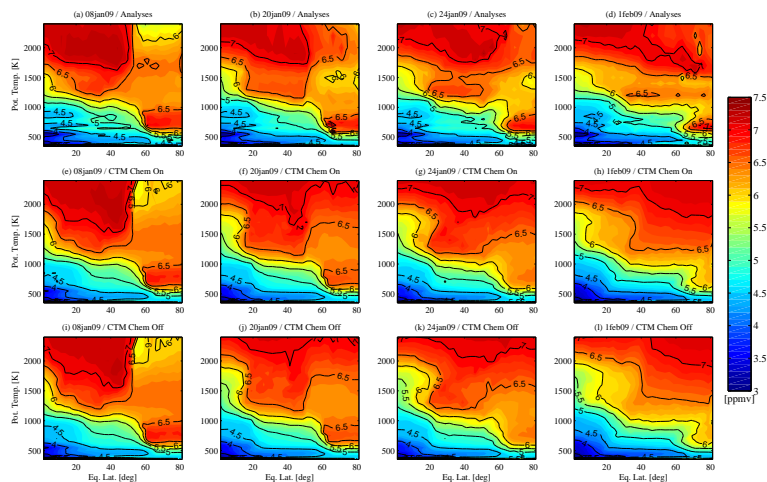


Fig. 8. Equivalent latitude-theta plots of water vapour fields at 1200 UTC (ppmv). Top row: BASCOE analyses; middle row: BASCOE CTM run (no assimilation), with chemistry; bottom row: BASCOE CTM run (no assimilation), no chemistry. Left column: 8 January 2009; middle left column: 20 January 2009; middle right column: 24 January 2009; right column: 1 February 2009. Red indicates relatively high values; blue indicates relatively low values.

[Title Page](#)
[Abstract](#)
[Introduction](#)
[Conclusions](#)
[References](#)
[Tables](#)
[Figures](#)
[Back](#)
[Close](#)
[Full Screen / Esc](#)
[Printer-friendly Version](#)
[Interactive Discussion](#)